Solar-Terrestrial Physics. 2024. Vol. 10. Iss. 3. P. 11–17. DOI: 10.12737/stp-103202402. © 2024 N.S. Meshalkina, A.T. Altyntsev. Published by INFRA-M Academic Publishing House

UDC 533.951, 537.868
DOI: 10.12737/stp-103202402

Received March 26, 2024
Accepted May 03, 2024

HEATING MANIFESTATIONS AT THE ONSET OF THE 29 JUNE 2012 FLARE

N.S. Meshalkina
Institute of Solar-Terrestrial Physics SB RAS, Irkutsk, Russia, nata@iszf.irk.ru

A.T. Altyntsev
Institute of Solar-Terrestrial Physics SB RAS, Irkutsk, Russia, altyntsev@iszf.irk.ru

Abstract. Analysis of GOES data for the SOL2012-06-29T04:09 flare, class C4.6, shows a thermal character of the energy release for several minutes before the impulsive stage. Plasma heating to temperatures above 10 MK leads to the appearance of plasma jets along open field lines and in large loops. This work examines the relationship between the heated plasma and the flare structure and its dynamics, using observations in the X-ray, extreme ultraviolet (EUV), and radio-wave ranges.

Particular attention is drawn to the detection of narrow-band fine temporal structures of radio emission before and after the impulsive stage of the flare in dynamic spectra. In the initial stage, broadband pulses in the decimeter range are observed which can be associated with the formation of thermal fronts in the jets. A series of super-bright drifting bursts in the centimeter range occurs after the end of the impulsive energy release in the flare core. Using data from the Siberian Solar Radio Telescope (5.7 GHz), we managed to localize the position of the source of the fine structure of drifting bursts at the remote footpoint of the large-scale flare loop.

Keywords: Sun, fine temporal structure, heating mechanisms, microwave bursts, coherent emission, thermal front, Neupert effect.

INTRODUCTION

It is well known that activity in the flare region in many cases manifests itself long before impulsive energy release in the main phase although it is not discussed in the widely accepted flare scenario — CSHKP [Carmichael, 1964; Sturrock, 1966; Hirayama, 1974; Kopp, Pneuman, 1976]. In the CSHKP model, there is a sudden release of magnetic energy in the corona due to magnetic reconnection, and a significant part of the energy is converted into kinetic energy of plasma and high-energy particles propagating along magnetic field lines. Electrons bombard the sufficiently dense chromosphere and transition zone, generating bremsstrahlung, which is observed in hard X-rays (HXR). As a result of this so-called chromospheric evaporation, plasma heats up, rises, and fills the loop, and we see soft X-rays (SXR) of hot plasma, generally at the top of the flare loop.

The Neupert effect [Neupert, 1968], to which corresponds the CSHKP flare model, explains the relationship between soft and hard X-rays. This effect suggests that non-thermal X-rays are generated directly by electron beams; and thermal soft X-rays, by hot plasma heated by the energy of the same electron beams. This hot plasma subsequently evaporates and accumulates in the corona (see, e.g., [Veronig et al., 2005]). While observations confirm the validity of the Neupert effect, previous statistical studies have shown that it can be disrupted in a significant proportion of events. When testing for delays between SXR and HXR bursts, it was found that about half of the events exhibit inconsistencies with this effect (for example, [Dennis, Zarro, 1993; McTiernan et al., 1999]).

A fairly obvious deviation from the Neupert effect occurs when SXR is observed before HXR, which may indicate the presence of thermal plasma that is heated not only by accelerated electrons [Acton et al., 1992]. According to [Dennis, 1988], the absence of energetic X-rays may be associated with the sensitivity of the threshold of HXR detectors; however, the studies [Benz et al., 1983; Jiang et al., 2006] show that this phenomenon cannot be explained by the lack of sensitivity to HXR [Benz, 2017]. Statistical study of 503 flares [Veronig et al., 2002a] has revealed that preheating occurs in SXR before the onset of the impulsive phase (detected in HXR) in more than 90 % of events. Moreover, Veronig et al. [2002b] have found no correlation between the duration of preheating and the intensity of the following flare. The data suggests that the Neupert effect is disrupted in more than half of the events, at least during the flare early phase, regardless of its intensity. SXR in the corona before the impulsive phase has also been reported in other studies [Caspi, Lin, 2010; Caspi et al., 2014, 2015]. These studies confirm that in order to explain SXR before the impulsive phase it is necessary to involve additional physical heating mechanisms, and not only accelerated electrons.

Hudson et al. [2021] have found that the plasma temperature exhibits common behavior at the earliest stages of solar flares of different power: plasma with a temperature 10–15 MK appears immediately, without any signs of a gradual increase in temperature, before an HXR burst. The hot radiation sources were located at footpoints of low loops. The authors have concluded that their heating is not explained by non-thermal electron fluxes.

Battaglia et al. [2009] have analyzed the pre-flare phase of several solar flares when an SXR rise was observed on the light curves from the RHESSI satellite,

but no HXR response was detected in the 12–25 keV channel. The authors attributed the heating to the heat conduction mechanism. In [Altyntsev et al., 2012], we have detected weak fluxes of non-thermal electrons in microwave observations, which were available for two of the four events considered. Thus, radio observations are a more sensitive method for detecting non-thermal electrons in the rarefied plasma of the solar corona.

Battaglia et al. [2023] have examined flares with hot sources from 10 to 16 MK, which appeared during the initial phase. The images obtained by STIX and AIA show that compact sources are not located at tops of loops, and heating is observed long before the occurrence of HXR.

In this paper, we analyze in detail the June 29, 2012 flare, using multiwave observations. The purpose of this work is to determine the relationship of a newly heated plasma with the flare structure and its dynamics at the early stage of the June 29, 2012 flare. This event is unusual in that during the early phase there is an outflow of thermal plasma with high temperatures up to 12 MK when there is still no response either in the radio range or in hard X-rays. Furthermore, a fine temporal structure was observed in the microwave radiation during the decay of the flare, which is unusual. Sources of subsecond pulses (SSPs) were located at a considerable distance from the main source of the flare energy release.

INSTRUMENTS AND METHODS

We have taken the data on spectral and spatial characteristics of extreme ultraviolet (EUV) radiation from the archive of the Solar Dynamic Observatory (SDO; [Pesnell et al., 2012]). We have used AIA images of the full solar disk, recorded every 12 s with a spatial resolution of 0.6″ [Lemen et al., 2012].

The light curves with a time resolution of 100 ms and 4 s for studying the temporal structure of X-rays, as well as images with a resolution of 4 s, were obtained from RHESSI data [Lin et al., 2002].

To record non-thermal emission, we have used data from the Siberian Solar Radio Telescope (SSRT), primarily one-dimensional (1D) scans of the solar disk at a frequency of 5.7 GHz with a time resolution of 14 ms [Grechnev et al., 2003; Meshalkina et al., 2012]. The beamwidth at half height was 17.8″ and 19.3″ in the east–west (EW) and north–south (NS) directions respectively. Short bursts lasting less than a second (subsecond pulses, SSPs) were detected using a sequence of SSRT scans. 1D scans were employed to study the fine temporal structure of the burst in intensity and polarization, as well as to localize SSP sources on the disk. The morphology and location of the background microwave burst of the source during the flare were explored from two-dimensional (2D) solar disk images captured by SSRT with a time resolution 2–3 min [Grechnev et al., 2003; Kochanov et al., 2013].

We have also employed data from the Badary Broadband Microwave Spectropolarimeter (BBMS) [Zhdanov, Zandanov, 2011] with an operating frequency range 4–8 GHz and a time resolution of 10 ms.

Dynamic spectra in the range of 15 to 2500 MHz were examined using HiRAS (Hiraiso Radio Spectrograph) data [Kondo et al., 1995].

We have also leveraged radio data from Nobeyama Radiopolarimeters (NoRP [Torii et al., 1979]), which measures intensity and circular polarization at six frequencies (1, 2, 3.75, 9.4, 17, and 35 GHz) with a time resolution of 1 s and 100 ms in flare mode. Spatial distribution of the radio burst and variations in the emission intensity were studied from sequences of images obtained by the Nobeyama Radioheliograph (NORH) at a frequency of 17 GHz with a spatial resolution of 10″ [Nakajima et al., 1994]. We have also used data from the Palehua Radio Telescope (Hawaii), which overlaps in time with the NoRP data. The telescope in Palehua is part of the USAF Radio Solar Telescope Network (RSTN) [Guidice et al., 1981], whose instruments measure intensity at eight frequencies (245, 410, 610, 1415, 2695, 4995, 8800, and 15400 MHz) with a resolution of 1 s.

OBSERVATIONS

The June 29, 2012 flare occurred at 04:09–04:16 UT (hereafter, Universal Time is used) in active region (AR) 11515; the flare class according to GOES is C4.6. Figure 1 presents light curves of the flare in X-rays, decimeter and microwave radiation.

During the initial phase of the flare, there was an increase in the SXR flux (data from GOES 0.5–8 Å, RHESSI in channels up to 20 keV) (see Figure 1, *a*, *b*) after 04:10. The plasma temperature reached 10 MK at 04:12, and then gradually increased to 15 MK. HXR (Figure 1, *d*) appeared at 04:13:20 (blue dash-dot line), i.e. the Neupert effect did not work in this event. In decimeter radiation in the RSTN channels (0.245–1.4 GHz), there was a short pulse at 04:12:47, twenty seconds before the main impulsive phase (Figure 1, *e*). This pulse was also observed by HiRAS in the 50–550 MHz range as a type III burst drifting to low frequencies (Figure 2).

The gyrosynchrotron microwave burst lagged behind HXR by 1.5 s, its spectral maximum was ~6–7 GHz, and the radiation flux reached 25 s.f.u.

EUV images show that energy release of the flare occurs in low loops (flare core in Figure 3) located at the footpoints of a large-scale loop and open field lines. A high loop is observed before the flare. At 04:09, compact brightenings appeared in the SDO/AIA images in the 304 Å channel [http://ru.iszf.irk.ru/~nata/120629/long.mp4]. This wavelength, at which relatively low temperatures (50000 K) are measured, was chosen because there were many overexposed frames in other AIA channels. A minute later, at 04:10, plasma began to flow along open field lines directed from west to east in the plane of the sky (Figure 4). With time, brightness of these plasma jets increased. Another jet emerged in a high closed loop and gradually reached the remote western footpoint of the loop.

The dynamics of the southern jet, along the trajectory of which the blue dashed line is drawn, is shown in the sequence of images in the 304 Å channel (see Figure 4). It can be seen from the brightness profiles (Figure 4) that during propagation of the hot plasma flow there is not a gradual increase characteristic of diffusion, but a steeping of ~ 6″ in size at the beginning of the jet, which can be interpreted as a quasistationary thermal front. Its velocity from 04:14:11 to 04:14:59 was ~400–500 km/s.

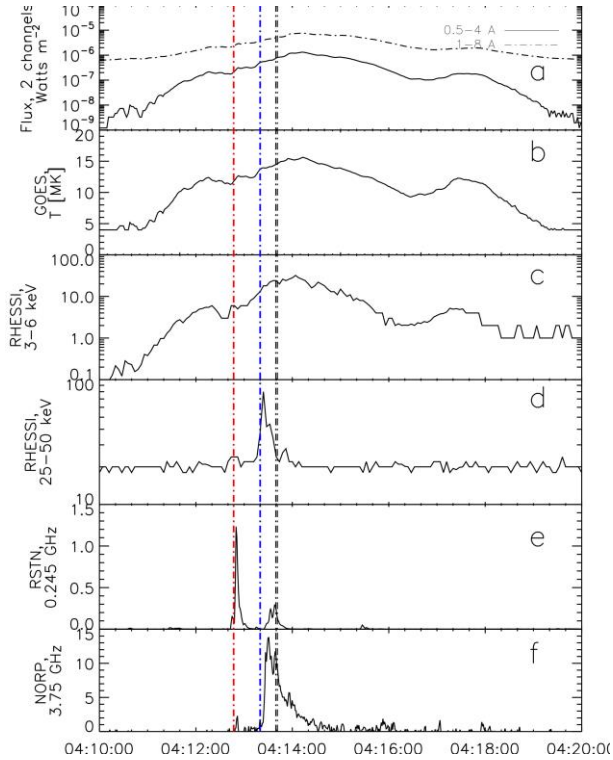

Figure 1. The June 29, 2012 event: *a* — GOES data, radiation fluxes (solid curve — 0.5–4 Å, dash-dot line — 1–8 Å); *b* — GOES data, temperature profile; *c*, *d* — time profiles of HXR in the 3–6, 25–50 keV RHESSI channels; *e* — intensity profile at a frequency of 0.245 GHz (RSTN); *f* — profile at 3.75 GHz (NORP). Appearance of a jet was detected around 04:10. Vertical dash-dot lines mark: red — time of the occurrence of decimeter bursts (see Figure 2); blue — rise in HXR at 04:13:20; black — interval with SSP (04:13:39.4–04:13:41.4)

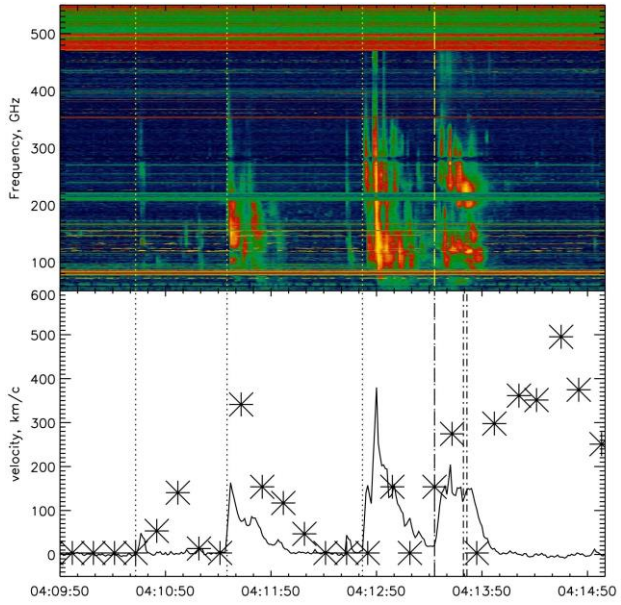

Figure 2. The June 29, 2012 event: *a* — dynamic spectrum (HiRAS); *b* — integral intensity of radio emission from 50 to 550 MHz (solid curve). Velocities of heat wave fronts propagating along open magnetic field lines (see Figure 4) are indicated by asterisks. Dotted lines mark the time of the beginning of radio bursts, the dash-dot line on both panels indicates the beginning of a burst of hard X-rays (04:13:23), two right dash-dot lines in the bottom panel bound the interval with SSP at a frequency of 5.7 GHz (04:13:39.4–04:13:41.4)

The EUV images made it possible to trace the structure of the jets at a distance of ~60″ from the flare core. Thermal wave fronts detached from the flare core four times; their velocities are designated in Figure 2, *b* by asterisks. Comparing the velocities of the fronts with the intensity of the emission integrated over frequency shows a high degree of time correlation between them.

The time of the formation of the fronts is close to that of detection of decimeter bursts.

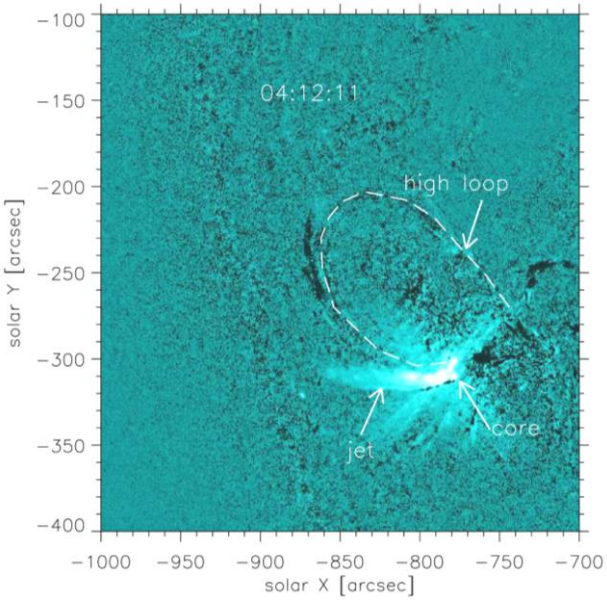

Figure 3. Large-scale structure of a flare region. Background is the difference between the images captured at 04:12:11 and 04:09:35 in the AIA/SDO 131 Å channel. The flare core, the jet (spray), and the high loop, along which another jet moved, are shown

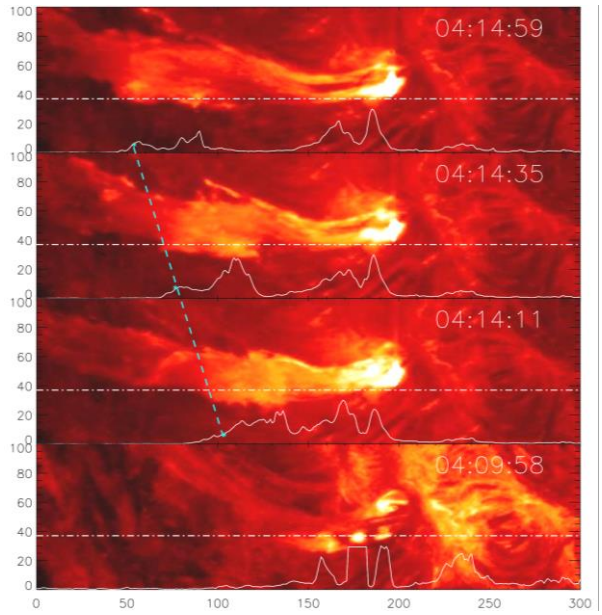

Figure 4. Images in the AIA/SDO 304 Å channel for the given time points. White dash-dot lines mark the horizontal cross-section of the image. The brightness profile along the cross-section is highlighted in white at the bottom of each panel. The blue dashed line connects fronts (brightness jumps) of the propagating jet. Along the X and Y axes, the values are given in pixels

Bursts of HXR and microwave radiation are observed during the impulsive phase of the flare. The spectral maximum of the microwave radiation of the flare is ~6–7 GHz, i.e. close to the frequency of SSRT observations. On maps of microwave radiation at a frequency of 5.7 GHz, to footpoints of a large-scale loop correspond two sources — core, or eastern (SE), and remote, or western (SW), indicated in Figure 5 by white contours. The behavior of brightness temperatures in these sources in the right-hand and left-hand polarizations is illustrated in Figure 6. In the core, microwave radiation begins at 04:13:20, i.e. approximately 3.5 min after the onset of plasma heating and the appearance of a jet. The degree of circular polarization of the flare core does not exceed 17 % according SSRT data. The front of microwave signal amplification in the remote source lags by 2.5 s, as previously shown in [Zhdanov, Zandanov, 2013]. The amplitude of the brightness temperature in the remote source is two times lower than in the core. At a frequency of 17 GHz, compact radiation sources (pink contours) are observed in both footpoints of the high loop (see Figure 5), whereas the remote source is weak and is confidently detected with 10 s delay. The HXR source is located near the center of the core brightness (orange contours in Figure 5, *b*).

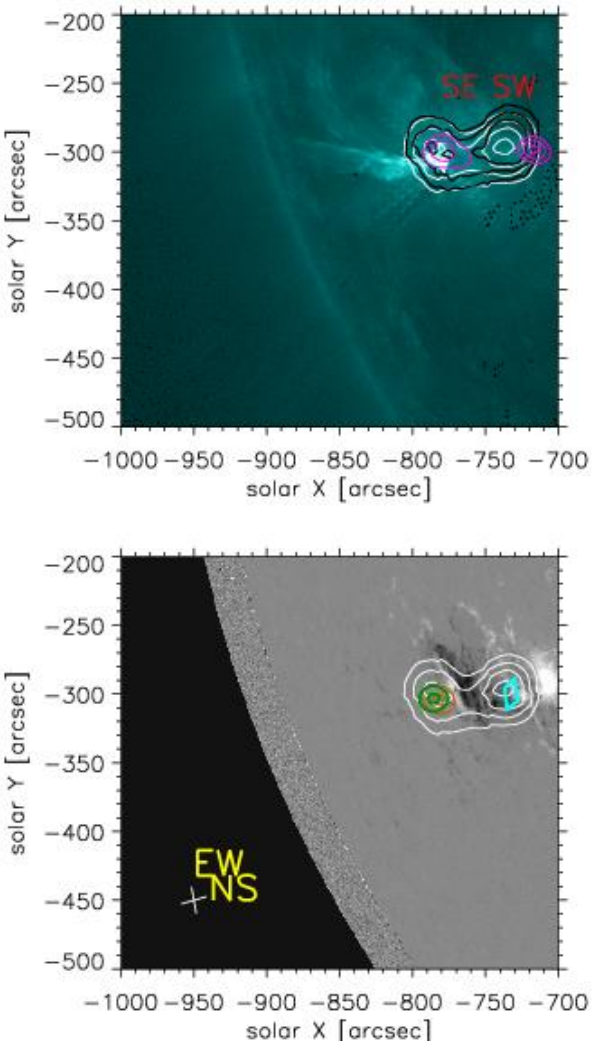

Figure 5. Image in AIA/SDO 131 Å channel at 04:13:47 with superimposed contours (*a*): white — distribution of brightness temperature (0.3, 0.5, 0.7, 0.9 of maximum) at 5.7 GHz at 04:13; black — distribution of brightness temperature in polarization at 5.7 GHz: solid — RCP (0.3, 0.5, 0.7 of maximum), dotted — LCP (0.3, 0.5, 0.7 of the minimum); pink — distribution of brightness temperature in intensity (0.5, 0.7, 0.9 of maximum) at a frequency of 17 GHz at 04:13:40; SE and SW — eastern (core) and western (remote) sources respectively. HMI/SDO magnetogram at 04:13:30 (*b*) with superimposed contours: white — the same as in panel *a*; orange — RHESSI data in the 25–50 keV channel (0.5, 0.9 of maximum); dark green — RHESSI data in the 6–12 keV channel (0.5, 0.9 of maximum); the blue frame marks the position of SSP sources; the white cross in the lower left corner is the SSRT antenna beamwidth

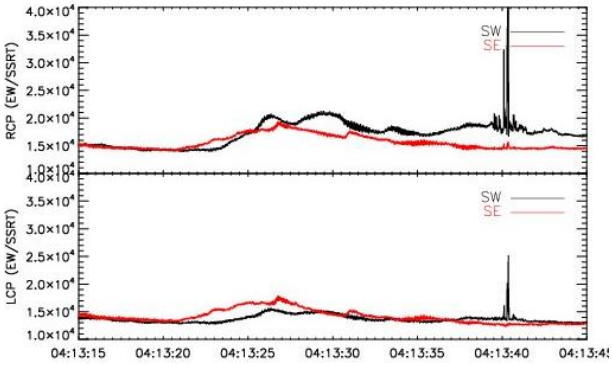

Figure 6. Brightness temperature profiles in microwave sources at a frequency of 5.7 GHz, measured by SSRT, in circular polarization: *a* — right-hand (RCP), *b* — left-hand (LCP). Red curves represent the flare core (SE); black curves, the remote source (SW)

A feature of the flare is a series of superbright SSPs at the SSRT receiving frequency, which occur during the decay of the microwave flare burst (see Figure 6). Brightness centers of SSP sources are located in the remote source, their position is indicated by the blue diamond in Figure 5, *b*. Note that the SSP radiation has a high degree of right-hand circular polarization — up to 100 % in some pulses.

Dynamic spectra with the fine temporal structure feature a variety of burst types: narrow-band driftless (with a bandwidth <1 GHz); drifting at velocities of ~15.2 GHz/s toward low frequencies (Figure 7); with an almost symmetrical drift toward high and low frequencies at velocities of 5.7 GHz/s and 11.3 GHz/s; a burst slowly drifting (2.9 GHz/s) toward high frequencies. The drifting bursts have different spectral bandwidths: from 0.89 to 1.4 GHz.

DISCUSSION

Observations suggest that distributions of flare energy release over channels (heating, acceleration of plasma and particle fluxes) differ significantly in dynamics and relative contribution. Events with a large contribution of energy to electron acceleration feature the Neupert effect. On the other hand, in some events (so-called thermal flares) there are no accelerated particles in HXR and microwave radiation (see, e.g., [Fleishman et al., 2015]). In the event under study, hot plasma with temperatures above 10 MK appears at the initial stage of the flare, and a burst of non-thermal electrons is observed a few minutes later. A feature of this event is the heating of plasma to an

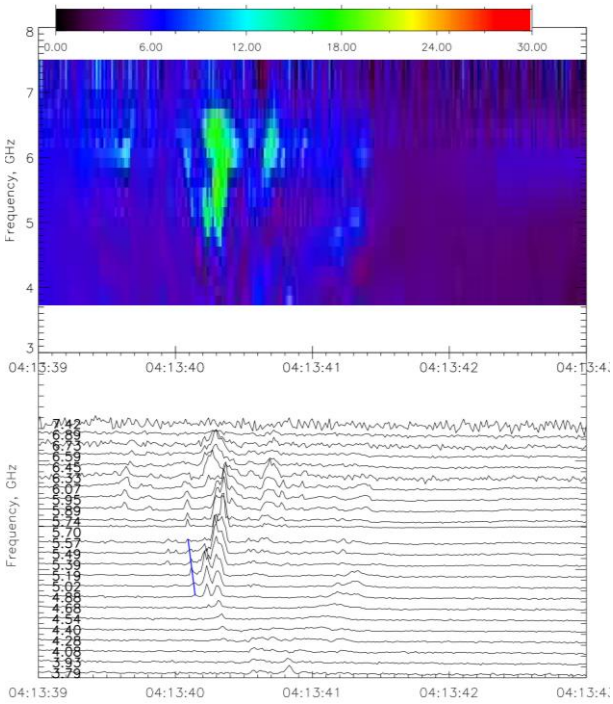

Figure 7. Dynamic spectrum (BBMS data) with fine temporal structure (top) and corresponding frequency time scanning (bottom, frequencies are indicated by numbers on the left). The blue line shows a burst shifting toward low frequencies

abnormally high temperature in low loops, as well as near footpoints of large-scale loops, which creates favorable conditions for studying heat and plasma propagation into the upper corona. Discussion of the mechanism of plasma heating near footpoints of high loops is beyond the scope of this work. We can mention the papers [Liu et al., 2013; Larosa, Moore, 1993; Somov et al., 1998] according to which superheated plasma is formed in turbulent current sheets.

The SDO/AIA images suggest that part of the heated plasma in the form of jets moves from the heating core along open field lines, and another part moves along high loops (closed in the field of view) toward remote footpoints. The behavior of EUV-brightness distributions was examined along the latitude-aligned open field line (see Figures 2, *b* and 4). For ~5 min from the appearance of the jet to the end of the impulsive phase, there were four sequentially propagating brightenings with a front width ~4–5 thousand km during plasma outflow. The fronts separated from the hot core of the flare and moved at velocities 300–500 km/s, which at a plasma temperature 10–15 MK are 30–40 times lower than the thermal velocity of electrons, but several times higher than the thermal velocity of ions.

Slowdown of spreading of hot electron bunches in cold plasma was previously observed in laboratory experiments [Ivanov et al., 1969; Ivanov, 1977; Manheimer, 1977]. In flares, this effect was first noted in [Batchelor et al., 1985; Rust et al., 1985]. A theoretical explanation for the formation of a heat jump between hot and cold plasmas moving at a velocity much lower than the thermal velocity of electrons was first proposed in [Ivanov et al., 1970]. Electrons scatter due to compensation of an outgoing charge by the counter flow of cold electrons since ions do not have time to move. Note that in the case of a jet in a radius-limited magnetic tube, an induction response to the fields of the counter flow also contributes to the neutralization of hot electron current [Hammer, Rostoker, 1970; Lee, Sudan, 1971]. The relative contribution and dynamics of these neutralization mechanisms are discussed in [Van den Oord, 1990].

The counter flow of cold electrons of sufficiently high intensity can be slowed down due to the appearance of abnormal resistance when current instabilities are excited. As demonstrated analytically and by numerical simulation [Ivanov et al., 1970; Brown et al., 1979; Smith, Lillequist, 1979; Bardakov, 1985; Arber, Melnikov, 2009], scattering of hot electrons can give rise to a stationary moving jump in the density of hot electrons, which can be interpreted as a wave of replacement, or heat front. Bardakov [1985] has shown that a stationary potential jump front is formed which moves at a velocity close to the ion-acoustic one. This result also remains valid for isothermal cold plasma. Results of laboratory experiments [Ivanov et al., 1969; Ivanov, 1977; Manheimer, 1977] also demonstrate velocities of heat wave propagation near the ion-acoustic wave velocity depending on the square root of the plasma ion mass.

Estimate the ion-acoustic wave velocity, using the formula [Aschwanden, 2004]

$$V_{\text{sound}} = 1.66 \cdot 10^4 \sqrt{T/\mu},$$

where μ is the ion-proton mass ratio. At μ(H)=1 and T=10–15 MK, V_{sound}=520–640 km/s. The observed velocities to 300–500 km/s agree with this estimate if it is remembered that the temperature decreases during expansion of the region with hot electrons when a heat wave appears. With decreasing temperature, the heat wave velocity decreases. The prolonged fourth wave is generated during the flare impulsive phase with high power energy release.

The thermal front serves as a barrier for low-energy electrons. High-energy part of the electrons in heated plasma can penetrate through the barrier and form a beam distribution behind it, which generates the observed drifting burst of decimeter radiation [Brown et al., 1979; Smith, Lillequist, 1979; Vlahos, Papadopoulos, 1979; Levin, Melnikov, 1993].

Fluxes of non-thermal electrons appear during the flare impulsive phase. At maximum hard X-ray signal, the index of the power law spectrum of electrons reaches a value of 3.8, which demonstrates the non-thermal nature of the burst. The microwave burst spectrum has a form characteristic of gyrosynchrotron emission. The maximum frequency is ~6 GHz. Comparing time profiles of 5.7 GHz radiation from the core and the remote source provides an estimate of the transit time of non-thermal electrons along a high loop at 2.5 s. Given a high loop length of 270″ (see Figure 3), we estimate the effective electron velocity at about 7.8×10^9 cm/s. When taking into account the spread of electron velocities in pitch angles and magnetic helicity, the estimate of electron velocity increases approximately twofold. In this case, the energy of non-thermal electrons generating gyrosynchronous emission in a remote source is at least 100 keV. Polarization of SSP in a remote source runs to 100 %.

Interestingly, subsecond pulses are observed in the remote source during the decay of the main burst in the flare core. The direction of SSP frequency drifts to high frequencies is consistent with the downward motion of emitting electrons to the western footpoint of the high loop. Presumably, some of the electrons are reflected since there is a case with reverse drift in microwave emission.

CONCLUSION

The June 29, 2012 flare saw no Neupert effect, i.e. this flare was a preheating event observed in soft X-rays before the impulsive phase, which was detected later in hard X-rays.

Heat waves are formed when the local plasma region is heated already in the flare initial phase and manifest themselves as jet eruption. The rate of thermal plasma outflow during jet eruption along an open magnetic field line (as a channel holding plasma) significantly exceeds the thermal velocity of ions and reaches values of the order of the ion-acoustic wave velocity.

The fine temporal structure in the microwave radiation was observed during the descending phase of the flare. It is noteworthy that SSP sources were far away from the main flare source, where the main energy release and hard X-ray emission occurred. SSPs are generally located in close proximity to the main energy release. The results demonstrate the importance of observations with spatial resolution.

The study was financially supported by RSF grant No. 22-12-00308. The section on the analysis of SSRT data and the fine structure (N.S.M.) was financially supported by the Ministry of Science and Higher Education of the Russian Federation with budgetary funding from Basic Research Program II.16.3.2 “Nonstationary and Wave Processes in the Solar Atmosphere”.

We are grateful to D.A. Zhdanov for his help in preparing BBMS data. We also thank the teams of the Solar Dynamic Observatory, GOES, HiRAS, Nobeyama Observatory, RHESSI, RSTN, and the ISTP SB RAS Radio Astrophysical Observatory for providing the data. The results were obtained using the Unique Research Facility “Siberian Solar Radio Telescope” [http://ckp-rf.ru/usu/73606/] and the equipment of Shared Equipment Center “Angara” [http://ckp-angara.iszf.irk.ru/].

REFERENCES

Acton L.W., Feldman U., Bruner M.E., Doschek G.A., Hirayama T., Hudson H.S., et al. The morphology of 20×10^6 K plasma in large non-impulsive solar flares. *Publ. Astron. Soc. Japan.* 1992, vol. 44, pp. L71– L75.

Altyntsev A.A., Fleishman G.D., Lesovoi S.V., Meshalkina N.S. Thermal to nonthermal energy partition at the early rise phase of solar flares. *Astrophys. J.* 2012, vol. 758, iss. 2, 138, 12 p. DOI: 10.1088/0004-637X/758/2/138.

Arber T.D., Melnikov V.F. Thermal fronts in flaring magnetic loops. *Astrophys. J.* 2009, vol. 690, iss. 1, pp. 238–243. DOI: 10.1088/0004-637X/690/1/238.

Aschwanden M.J. *Physics of the Solar Corona: An Introduction.* Springer-Verlag; Praxis, 2004, 842 p.

Bardakov V.M. Structure of a thermal wave in a collisionless plasma. *Soviet Journal of Plasma Physics*. 1985, vol. 11, pp. 699–703.

Batchelor D.A., Crannell C.J.; Wiehl H.J., Magun A. Evidence for collisionless conduction fronts in impulsive solar flares. *Astrophys. J.* 1985, vol. 295, pp. 258–264. DOI: 10.1086/163370.

Battaglia M., Fletcher L., Benz A.O. Observations of conduction driven evaporation in the early rise phase of solar flares. *Astron. Astrophys.* 2009, vol. 498, iss. 3, pp. 891–900. DOI: 10.1051/0004-6361/200811196.

Battaglia A.F., Hudson H., Warmuth A., Collier H., Jeffrey N.L.S., Caspi A., et al. The existence of hot X-ray onsets in solar flares. *Astron. Astrophys*. 2023, vol. 679, A139, 14 p. DOI: 10.1051/0004-6361/202347706.

Benz A.O. Flare observations. *Living Rev. Sol. Phys*. 2017, vol. 14, 2, 59 p. DOI: 10.1007/s41116-016-0004-3.

Benz A.O., Barrow C.H., Dennis B.R., Pick M., Raoult A., Simnett G. X-ray and radio emissions in the early stages of solar flares. *Solar Phys*. 1983, vol. 83, pp. 267–283. DOI: 10.1007/ BF00148280.

Brown J.C., Melrose D.B., Spicer D.S. Production of a collisionless conduction front by rapid coronal heating and its role in solar hard X-ray bursts. *Astrophys. J.* 1979, vol. 228, pp. 592–597. DOI: 10.1086/156883.

Carmichael H.A Process for flares. *The Physics of Solar Flares: Proc. AAS-NASA Symposium*. 1964, pp. 451–456.

Caspi A., Lin R.P. RHESSI line and continuum observations of super-hot flare plasma. *Astrophys. J.* 2010, vol. 725, iss. 2, pp. L161–L166. DOI: 10.1088/2041-8205/725/2/L161.

Caspi A., Krucker S., Lin R.P. Statistical properties of super-hot solar flares. *Astrophys. J.* 2014, vol. 781, 43. 11 p. DOI: 10.1088/0004-637X/781/1/43.

Caspi A., Shih A.Y., McTiernan J.M., Krucker S. Hard X-ray imaging of individual spectral components in solar flares. *Astrophys. J.* 2015, vol. 811, iss. 1, L1, 8 p. DOI: 10.1088/2041-8205/811/1/L1.

Dennis B.R. Solar flare hard X-ray observations. *Solar Phys*. 1988, vol. 118, iss. 1-2, pp. 49–94. DOI: 10.1007/BF00148588.

Dennis B.R., Zarro D.M. The Neupert effect: What can it tell up about the impulsive and gradual phases of solar flares. *Solar Phys*. 1993, vol. 146, pp. 177–190. DOI: 10.1007/BF00662178.

Fleishman G.D., Nita G.M., Gary D.E. Energy partitions and evolution in a purely thermal solar flare. *Astrophys. J.* 2015, vol. 802, iss. 2, 122, 13 p. DOI: 10.1088/0004-637X/802/2/122.

Grechnev V.V., Lesovoi S.V., Smolkov G.Ya., Krissinel B.B., Zandanov V.G., Altyntsev A.T., Kardapolova N.N., Sergeev R.Y., Uralov A.M., Maksimov V.P., Lubyshev B.I. The Siberian Solar Radio Telescope: The current state of the instrument, observations, and data. *Solar Phys*. 2003, vol. 216, pp. 239–272. DOI: 10.1023/A:1026153410061.

Guidice D.A., Cliver E.W., Barron W.R., Kahler S. The Air Force RSTN System. *Bull. American Astronomical Society.* 1981, vol. 13, p. 553.

Hammer D.A., Rostoker N. Propagation of high current relativistic electron beams. *Physics of Fluids*. 1970, vol. 13, pp. 1831–1850. DOI: 10.1063/1.1693161.

Hirayama T. Theoretical model of flares and prominences. I: Evaporating flare model. *Solar Phys.* 1974, vol. 34, iss. 2, pp. 323–338. DOI: 10.1007/BF00153671.

Hudson H.S., Simões P.J.A., Fletcher L. Hayes L.A., Hannah I.G. Hot X-ray onsets of solar flares. *Monthly Notices of the Royal Astronomical Society*. 2021, vol. 501, iss. 1, pp. 1273–1281. DOI: 10.1093/mnras/staa3664.

Ivanov A.A. *Physics of Strong Disturbed Plasma.* Moscow, Atomizdat Publ., 1977, 352 p. (In Russian).

Ivanov A.A., Kozorovitskii L.L., Rusanov B.D. Propagation of heat in plasma along the magnetic field (substitution wave). *Reports of USSR Academy of Sciences*. 1969, vol. 184,

pp. 811–814. (In Russian).

Ivanov A.A., Rusanov V.D., Sagdeev R.Z. Electron shock waves in a collisionless plasma. *Soviet JETP Lett.* 1970, vol. 2, p. 20.

Jiang Y.W., Liu S., Liu W., Petrosian V. Evolution of the loop-top source of solar flares: Heating and cooling processes. *Astrophys. J.* 2006, vol. 638, pp. 1140–1153. DOI: 10.1086/498863.

Kochanov A.A., Anfinogentov S.A., Prosovetsky D.V., Rudenko G.V., Grechnev V.V. Imaging of the solar atmosphere by the Siberian Solar Radio Telescope at 5.7 GHz with an enhanced dynamic range. *Publ. Astron. Soc. Japan.* 2013, vol. 65, no. SP1, article id. S19, 12 p. DOI: 10.1093/pasj/65.sp1.S19.

Kondo T., Isobe T., Igi S., Watari Sh., Tokumaru M. The Hiraiso Radio Spectrograph (HiRAS) for monitoring solar radio bursts. *Journal of the Communications Research Laboratory.* 1995, vol. 42, p. 111.

Kopp R.A., Pneuman G.W. Magnetic reconnection in the corona and the loop prominence phenomenon. *Solar Phys*. 1976, vol. 50, pp. 85–98. DOI: 10.1007/BF00206193.

Larosa T.N., Moore R.L. A Mechanism for bulk energization in the impulsive phase of solar flares: MHD turbulent cascade. *Astrophys. J.* 1993, vol. 418, p. 912. DOI: 10.1086/173448.

Lee R., Sudan R.N. Return current induced by a relativistic beam propagating in a magnetized plasma. *Physics of Fluids*. 1971, vol. 14, pp. 1213–1225. DOI: 10.1063/1.1693588.

Lemen J.R., Title A.M., Akin D.J., Boerner P.F, Chou C., Drake J.F., Duncan D.W., Edwards Ch.G., et al. The Atmospheric Imaging Assembly (AIA) on the Solar Dynamics Observatory (SDO). *Solar Phys*. 2012, vol. 275, no. 1-2, pp. 17–40. DOI: 10.1007/s11207-011-9776-8.

Levin B.N., Melnikov V.F. Quasi-linear model for the plasma mechanism of narrow-band microwave burst generation. *Solar Phys*. 1993, vol. 148, iss. 2, pp. 325–340. DOI: 10.1007/ BF00645093.

Lin R.P., Dennis B.R., Hurford G.J., Smith D.M., Zehnder A., Harvey P.R., Curtis D.W., Pankow D., Turin P., et al. The Reuven Ramaty High-Energy Solar Spectroscopic Imager (RHESSI). *Solar Phys*. 2002, vol. 210, pp. 3–32. DOI: 10.1023/A:102 2428818870.

Liu S., Li Y., Fletcher L. Impulsive thermal X-ray emission from a low-lying coronal loop. *Astrophys. J.* 2013, vol. 769, iss. 2, 135, 10 p. DOI: 10.1088/0004-637X/769/2/135.

Manheimer W.M. Energy flux limitation by ion acoustic turbulence in laser fusion schemes. *Physics of Fluids.* 1977, vol. 20, pp. 265–270. DOI: 10.1063/1.861863.

McTiernan J.M., Fisher G.H., Li P. The solar flare soft X-ray differential emission measure and the Neupert effect at different temperatures. *Astrophys. J.* 1999, vol. 514, pp. 472–483. DOI: 10.1086/306924.

Meshalkina N.S., Altyntsev A.T., Zhdanov D.A. Study of flare energy release using events with numerous type III-like bursts in microwaves. *Solar Phys.* 2012, vol. 280, iss.2, pp. 537–549. DOI: 10.1007/s11207-012-0065-y.

Nakajima H., Nishio M., Enome S., Shibasaki K., Takano T., Hanaoka Y., Torii C., et al. The Nobeyama Radioheliograph. *Proc. IEEE.* 1994, vol. 82, p. 705.

Neupert W.M. Comparison of solar X-ray line emission with microwave emission during flares. *Astrophys. J.* 1968, vol. 153, p. L59.

Pesnell W.D., Thompson B.J., Chamberlin P.C. The Solar Dynamics Observatory (SDO). *Solar Phys*. 2012, vol. 275, iss. 1-2, pp. 3–15. DOI: 10.1007/s11207-011-9841-3.

Rust D.M., Simnett G.M., Smith D.F. Observational evidence for thermal wave fronts in solar flares. *Astrophys. J.* 1985, vol. 288, pp. 401–409. DOI: 10.1086/162804.

Smith D.F., Lillequist C.G. Confinement of hot, hard X-ray producing electrons in solar flares. *Astrophys. J.* 1979, vol. 232, pp. 582–589. DOI: 10.1086/157316.

Somov B.V., Kosugi T., Sakao T. Collisionless three-dimensional reconnection in impulsive solar flares. *Astrophys. J.* 1998, vol. 497, iss. 2, pp. 943–956. DOI: 10.1086/305492.

Sturrock P.A. Model of the high-energy phase of solar flares. *Nature.* 1966, vol. 211, iss. 5050, pp. 695–697. DOI: 10.1038/ 211695a0.

Torii C., Tsukiji Y., Kobayashi S., Yoshimi N., Tanaka H., Enome S. Full-automatic radiopolarimeters for solar patrol at microwave frequencies. *Proc. of the Research Institute of Atmospherics*. Nagoya University, 1979, vol. 26, pp. 129–132.

Van den Oord G.H.J. The electrodynamics of beam/return current systems in the solar corona. *Astron. Astrophys.*1990, vol. 234, no. 1-2, pp. 496–518.

Veronig A., Vršnak B., Dennis B.R., Temmer M., Hanslmeier A., Magdalenić J. Investigation of the Neupert effect in solar flares. I. Statistical properties and the evaporation model. *Astrophys. J.* 2002a, vol. 392, pp. 699–712. DOI: 10.1051/0004-6361:20020947.

Veronig A., Vršnak B., Temmer M., Hanslmeier A. Relative timing of solar flares observed at different wavelengths. *Solar Phys*. 2002b, vol. 208, iss.2, pp. 297–315. DOI: 10.1023/A: 1020563804164.

Veronig A.M., Brown J.C., Dennis B.R., Schwartz R.A., Sui L., Tolbert A.K. Physics of the Neupert effect: Estimates of the effects of source energy, mass transport, and geometry using RHESSI and GOES data. *Astrophys. J.* 2005, vol. 621, pp. 482–497. DOI: 10.1086/427274.

Vlahos L., Papadopoulos K. Collective plasma effects associated with the continuous injection model of solar flare particle streams. *Astrophys. J.* 1979, part 1, vol. 233, oct. 15, pp. 717–726. DOI: 10.1086/157433.

Zhdanov D.A., Zandanov V.G. Broadband microwave spectropolarimeter. *Central European Astrophys. Bull.* 2011, vol. 35, p. 223.

Zhdanov D.A., Zandanov V.G. First microwave spectral observation of two sources during the solar flare event. *BSHFF-2013. Section A: Astrophysics and Physics of the Sun.* 2013, pp. 70–71. (In Russian).

URL: http://ru.iszf.irk.ru/~nata/120629/long.mp4 (accessed March 26, 2024).

URL: http://ckp-rf.ru/usu/73606/ (accessed March 26, 2024).

URL: http://ckp-angara.iszf.irk.ru/ (accessed March 26, 2024).

This paper is based on material presented at the 19th Annual Conference on Plasma Physics in the Solar System, February 5–9, 2024, IKI RAS, Moscow.

Original Russian version: Meshalkina N.S., Altyntsev A.T., published in Solnechno-zemnaya fizika. 2024. Vol. 10. No. 3. P. 13–20. DOI: 10.12737/szf-103202402 © 2024 INFRA-M Academic Publishing House (Nauchno-Izdatelskii Tsentr INFRA-M)

How to cite this article

Meshalkina N.S., Altyntsev A.T. Heating manifestations at the onset of the 29 June 2012 flare. *Solar-Terrestrial Physics*. 2024. Vol. 10. Iss. 3. P. 11–17. DOI: 10.12737/stp-103202402.